

Quantum Circuits, Feature Maps, and Expanded Pseudo-Entropy: A Categorical Theoretic Analysis of Encoding Real-World Data into a Quantum Computer

Andrew Vlasic

Deloitte Consulting LLP

(Dated: February 27, 2025)

This manuscript proposes a new and novel numerical method to determine the efficacy of an encoding scheme to map real-world data into a quantum circuit. The method calculates the Shannon entropy of each of the data points from a point-cloud, hence, samples from an embedded manifold, and calculates the expanded concept of pseudo-entropy applied to each respective quantum operator that comes from a given quantum feature map, and not the density operator. In the recent decade, there has been a continuous advancement of translating machine learning into a quantum circuit with many promising results. For quantum machine learning, a major underlying question is how to encode real-world data into a quantum circuit without losing information and adding noise. A few notable methods derived are expressibility, where the distribution of the output of states from the circuit are compared against the Haar probability measure with information theoretic techniques, and expressivity, a method that maps the expectation of a quantum circuit to the space of complex functions via a partial Fourier series, noting that more intricate the function the more expressive, and using the symmetry embedded within the data to derive a quantum feature map. The proposed pseudo-entropy method is discussed to and empirically shown to generalize these methods. Furthermore, this method is argued to also generalize symmetric quantum feature maps. The discussions and arguments are a reasonable basis for understanding the connections but require deeper mathematical analysis.

I. INTRODUCTION

The goal of this paper is to describe an analytic extension of von Neumann entropy in which the domain is the space of special unitary operators, denoted as *pseudo-entropy*. Pseudo-entropy is shown to be informative and a mathematically sound approach to determine whether information from real-world data is transferred to and retained in a quantum circuit within the context of quantum machine learning. The manuscript focuses on quantum encoding techniques, also known as quantum feature maps. To display the technique, empirical analysis is applied to toy data and real-world data, where the real-world data has a binary classification task and the performance of the quantum statistical models are compared to the pseudo-entropy. The analysis with the real-world data shows that further generalization of the method from quantum feature maps to different QML models based on pseudo-entropy is needed to provide a new pathway to design more efficient QML models.

Taking inspiration from information theory, the perspective that each data point in the point-cloud has ‘energy’ and this ‘energy’ is transferred to a quantum gate, or special unitary operator. By using a particular invertible mapping from real data domains to an n -simplex, one can associate Shannon entropy with each data point. We propose that pseudo-entropy can be associated with *quantum encodings* as a measure of information; observe that this proposed analysis is quite different than von Neumann entropy which considers the density matrix of a pure quantum state. The idea is then to design quantum encodings that map classical data to unitary circuits in a way that retains some similarity to Shannon information. We use two different methods to measure this similarity,

namely the Spearman and Xicor correlation functions. Thus, the strength of the relationship between these two entropy values tests how well information is transferred.

Within this framework, the point-cloud is assumed to represent a sampling of points on an embedded smooth manifold; this assumption is not too restrictive as the smoothing out of rough corners on the manifold either deletes little information or adds a little noise.

With a few examples, we compare the correlations coefficients between each quantum feature map and entropy of data against the average performance of the binary statistical models with the respective quantum encoding. The empirical results are mixed, indicating further mathematical analysis is required to gauge the efficacy of a quantum statistical model trained with an encoding scheme. Given the complexity that extra gates add to the algorithm, this result is not surprising.

To mathematically describe the relationship between the two entropies, techniques from category theory are applied to describe the flow of information. The entropy of the data and the pseudo-entropy of the encoding scheme with respect to the data are shown to be equivalent through the existence of a natural transformation from the composition of functors, where these functors are faithful. Moreover, these techniques assist in crafting which set of questions one may ask to further derive a generalization of technique.

Finally, the technique is argued to generalize standard techniques in the QML community to gauge the efficacy of an encoding technique, and potentially, a full quantum circuit.

The rest of the paper is organized as follows. Section II discusses encoding schemes in detail and describes three well-used quantum feature maps. The section ends by

describing the difficulty of analyzing a quantum feature map and argues that the analysis should be conducted on the group of quantum gates, the group of special unitary matrices. Section III gives brief overviews of information geometry and category theory in order to establish a foundation for the rest of the paper. Section III C describes in detail the derivation of the analytic extension of von Neumann entropy applied to a given quantum feature map. Section IV describes the proposed technique in detail with motivating toy examples and describes through methods in category theory the connection between entropy values of a point-cloud and the respective pseudo-entropy values with a given quantum feature map. Section IV C formalizes the technique to a given manifold and argues the technique generalizes expressibility, expressivity, and symmetric encoding, all which are described before each argument. Finally, Section V summarizes the paper and gives shortcomings of the paper, describing areas of future research.

II. OVERVIEW OF FEATURE MAPS AND ANALYSIS

Encoding real-world data into a quantum circuit is, on the surface, a straightforward question to answer with various quantum feature maps to chose for application. However, once one starts asking deeper questions about quantum feature maps, the question of encoding real-world data into a quantum circuit becomes intricate and quite convoluted.

This section gives an overview of various quantum feature maps, the status of the research, and lastly, deeper questions one may ask and the difficulty of answering each.

A. Feature Maps and Analysis

There have been many proposed quantum feature maps [1–4], the basis of which embed data as a phase, embed data as an angle, embed data as an amplitude, where some maps have pairwise entanglement between features, and combinations therein. The intuition behind quantum feature maps varies from leveraging the physics to extract the frequency of the representative binary of the number (see [3] for an example with a binary representing the position in the array), translating an array into the structure of quantum observables [1], to neural network architecture which use pairwise entanglement as a layer to incorporate the non-locality behavior of qubits (see the many examples in [2]), thereby leveraging quantum mechanics to map data points to a higher dimensional complex Hilbert space.

For completeness the IQP, angle, and amplitude encoding feature maps are described, as these encoding schemes are well-applied. The feature maps are described in general, with IQP having many different forms and

combinations of layers. For the experiments in the paper, the specific IQP schemes applied are described in detail.

a. Angle Angle encoding [5, 6] is an intuitive mapping where each entry of the data point, say x , are the angles of a rotation operator. Specifically, for a Pauli operator σ , that is $\sigma \in \{X, Y, Z\}$, $R_\sigma(\theta) = \exp(-i\frac{\theta}{2}\sigma)$ is the form of a rotation operator. For the angle encoding scheme, it is typical for $\sigma = X$. Thus, for X_i the Pauli- X gate acting on the i^{th} qubit and x_i the i^{th} entry of the data point, the encoded operator has the form

$$U(x) = \bigotimes_{l=1,2,\dots,n} \exp\left(-i\frac{x_l}{2}X_l\right). \quad (1)$$

This feature map has been noted to not take full advantage of quantum mechanics as there are no gates that create entanglement.

b. IQP The authors Havlíček et al. [1] derived the IQP feature map, where the authors assume a data point $x \in (0, 2\pi)^n$. Taking Z_l as the Pauli- Z gate acting on the l^{th} qubit, denote the operator

$$U_Z(x) = \exp\left(\sum_{i=1}^n x_i Z_i + \sum_{i=1}^n \sum_{j=1}^n (\pi - x_i)(\pi - x_j) Z_i Z_j\right), \quad (2)$$

, and in general this operator has the form $U_\Phi(x) = \exp\left(\sum_{S \subset \{1,2,\dots,n\}} \Phi_S(x) \prod_{i \in S} Z_i\right)$. For the Hadamard gate, H , IQP has the form

$$U(x) = U_Z(x) H^{\otimes n} U_Z(x) H^{\otimes n}. \quad (3)$$

For the experiments in this paper, a version of Equation 3 is applied and follows closer the derived encoding scheme in Bremner, Montanaro, and Shepherd [7]. Particularly, the phase gate and controlled phase gate are applied,

$$p(\theta) = \begin{bmatrix} 1 & 0 \\ 0 & \exp(i\theta) \end{bmatrix}, \quad (4)$$

is applied as a single and controlled gate. Observe, though, that the phase gate is a phase of off the Paul Z rotational gate, $p(\theta) = \exp(i\frac{\theta}{2} R_z(\theta))$. Furthermore, one may show that the controlled phase gate is a phase factor off of the operator $R_{zz}(-\theta)R_z(\theta) \otimes R_z(\theta)$. For simplicity of the circuit, controlled phase gates and phase gates are the only variational circuits applied in the experiments. Since a control gate is difficult to define as an operator, take $CP(\theta, k, j)$ as the the controlled phase gate on the k^{th} qubit conditioned on the j^{th} qubit. Finally, denote the **IQP** encoding scheme as the application of the operator

$$H^{\otimes n} \prod_k \prod_{j>k} CP(\theta, k, j) \prod_k P(x_k) H^{\otimes n}, \quad (5)$$

where $\pi_{k,j} := (\pi - x_k)(\pi - x_j)$.

However, since the construction of the IQP encoding in Equation 5 scheme may be seen as a hyperparameter, as well as general IQP, we define the **IQP SO** encoding scheme as

$$\prod_k \prod_{j>k} \text{CP}(\theta, k, j) \prod_k P(x_k), \quad (6)$$

ergo, IQP without the Hadamard gate layers, and the **IQP FL** encoding scheme

$$\text{CP}(\theta, k, j) \prod_k P(x_k) H^{\otimes n} \prod_k \prod_{j>k} \text{CP}(\theta, k, j) \prod_k P(x_k) H^{\otimes n}, \quad (7)$$

which is IQP with a re-upload of the data point.

c. Amplitude Amplitude encoding [3, 8] takes a data point x of the form $\sum_{i=1}^n |x_i|^2 = 1$, with $n = 2^m$ for $m \in \mathbb{N}$, into a binary tree structure. The partitions are entries of the data point and recursively split in half and built back by locally normalizing; the local normalization is reminiscent of Bayes. Given the ambiguity of the construction, consider the amplitude encoding of the simple example of the data point $(.17, .4, .23, .2)$. This data point will be decomposed to craft a circuit in order to create the pure state $\sqrt{.17} |00\rangle + \sqrt{.40} |10\rangle + \sqrt{.23} |01\rangle + \sqrt{.20} |11\rangle$. The binary tree and subsequent circuit is given in Figure 1. For simplicity of the quantum circuit for amplitude encoding, we define the rotational gate $\tilde{R}_y(\alpha) = R_y(2 \cdot \arccos(\alpha))$.

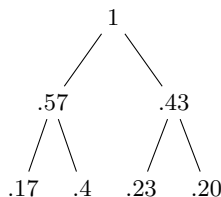


FIG. 1: This is the binary tree decomposition of the data point $(.17, .4, .23, .2)$.

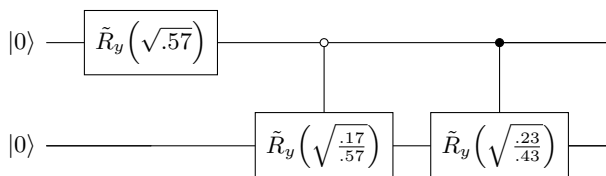


FIG. 2: This is the respective circuit of the binary tree in Figure 1.

The authors in [3] derive another technique, which they denote as divide-and-conquer, to encode the amplitude of a data point. Given the intricacy of the algorithm the description will be left out, and the reader is encouraged to read the paper.

Given the variety of quantum feature maps, there has been an effort to analyze encoding schemes through experimentation [9, 10], representing quantum feature maps in different forms and approximations [2, 4, 11], and, in the special case of symmetric data, Lie algebras mathematically backed with category theory [12]. The majority of the experiments are classification problems where the efficacy of the statistical model is considered.

Vlasic and Anh [10] derived a computational friendly technique to calculate the Betti numbers [13] for the geometry generated from the quantum feature map; Betti numbers are a topological analysis technique to visualize the topology of a point-cloud [14]. With a synthetic toy dataset of a two dimensional donut and three well-used quantum feature maps, Vlasic and Anh displayed the vast topological differences between all of the encoding schemes, and vast differences of each scheme and the original data, showing the need for deeper analysis.

Currently, the most influential work comes from Schuld, Sweke, and Meyer [4], who considered a partial Fourier series of a given circuit to calculate the “expressivity” of the method, which may yield intricacies of a quantum feature map and the ability of the map to span the higher dimensional Hilbert space. Ergo, entanglement, and as a consequence, the depth of the non-locality is displayed in their proposed Fourier expansion. The Fourier expansion serves as a basis to understand how intricate the encoding scheme is with respect to leveraging quantum characteristics. Further a highly influential method comes from Sim et al. [2] on the method of “expressibility”, which compares the Haar probability measure and against the distribution of states produces by a circuit. Both expressivity and expressibility implicitly have entanglement increase their positive scores; it should be noted that entanglement has been argued to yield an advantage, see Schatzki et al. [15].

B. The Difficulty of Analyzing Feature Maps

The techniques noted in Subsection II A give abundant insights into individual quantum feature maps, and circuits in general, by calculating the intricacies of the aggregated circuit output. However, these insights are limited and lack a full mathematical description for a complete rigorous analysis. To the contrary, given a symmetric point-cloud, or symmetric embedded manifold, the results of Meyer et al. [12] assists with the complete derivation of an information preserving quantum feature map through symmetry.

It is proposed that the focus of analyzing general encoding schemes should establish a theoretical assurance of full information retention, or at least minimal retention of ‘important’ information. Of course, the concept of information is not well-defined since there are different perspectives of what is implied by information. To demonstrate different perspectives, first observe that a given point-cloud represents samples from an embedded

manifold in \mathbb{R}^n , call it M . Now, a quantum feature map, say f , takes points in M to a special unitary operator with a final size of $2^k \times 2^k$. Ergo, the space of special unitary operators, denoted as $SU(2^k)$ where 2^k is assumed to be the space $(\mathbb{C}^2)^{\otimes k}$. Hence, a quantum feature map is a morphism of the form $f : M \rightarrow SU(2^k)$. From here one may stop and analyze questions about retention of topology structure, including geodesic flows, retention of algebraic structure, and or the retention of information via information theory.

Notice that the vast majority of techniques consider the expected output of the quantum circuit, adding an extra mapping step beyond the space $f(M) \subset SU(2^k)$. This extra step is difficult to describe as a flow of information since it is the range of each individual function, ergo, the expected output of a quantum circuit. Hence, the extra step has a large potential of losing information since the functions themselves are not analyzed.

Therefore, a quantum feature map is a morphism where information is either topology [16, 17], geodesic flows [18, 19], algebraic structure [18, 20], or information geometry [21, 22]. Information retention is then keeping the structure of a commutative geometry the ‘same’ structure in the noncommutative geometry [18] of $SU(2^k)$. Therein lies the difficulty, comparing commutative structures to noncommutative structures. However, the areas of commutative and noncommutative geometry are well-studied with a deep and rich literature.

This manuscript focuses on the information geometry of the an embedded smooth manifold and the respective subspace of operators in the space of special unitary operators.

III. MATHEMATICAL FOUNDATION OF ANALYTIC TOOLS

This section gives an overview of the accompanying mathematical frameworks to analyze quantum feature maps and quantify how well maps are able to retain information. Particularly, to capture the flow of information and connect different flows, an overview of category theory is given. Also, since the information perspective of entropy is the focus, an overview of information geometry is also given. For brevity, the overviews are given with minimal information.

Finally, Section III C gives the derivation of an analytic extension of von Neumann entropy [23]. We call this extension *pseudo-entropy* to keep the definition similar to that of the literature. The concept of pseudo-entropy is the basis for connecting classical entropy of a data point to the entropy of the operator, as will be motivated and discussed in future sections.

A. Information Geometry

To extract information from data in a given point-cloud one must first ask what one means by information, as noted in Subsection II B. Information theory has a well-established foundation for measuring information and information loss, with vast applications in physics [24, 25]. For a discrete distribution $\mathbf{p} = (p_0, p_1, \dots, p_n)$ recall the entropy of this distribution is

$H(\mathbf{p}) = -\sum_{i=0}^n p_i \log(p_i)$, which measures, for example, the current disorder of a system.

With our point-cloud given a prior to a particular task, and putting emphasis that quantum feature maps are an element-wise mapping, the entropy of individuals points will be the basis of information. The safe assumption of the point-cloud is that it is a subset of \mathbb{R}^d , with only very special cases being a subset of an n -simplex, given by

$$\Delta^n := \left\{ x \in \mathbb{R}^{n+1} : \sum_i x_i = 1 \text{ and } x_i > 0 \forall i \right\}.$$

However, there exists diffeomorphisms, call one g , where the mapping $g : \Delta^n \rightarrow \Delta^{d+1}$ ensures the geometric structure of the point-cloud is preserved.

To add further context and mathematical guarantees, the results from information geometry [21] yields deeper insight into the tools used to extract information. In fact, for a collection of finite distributions, one may see that these distributions can be rewritten as an exponential family of probability density functions. With this manifold the Riemannian metric is the Fisher information matrix, and the Fisher information matrix is a unique invariant metric. Moreover, given that other functions exist to calculate information other than entropy, in general, define *f-divergence* is a convex differentiable function with $f(1) = 0$ with divergence defined as $D_f(\mathbf{p}||\mathbf{q}) = \sum p_i f\left(\frac{q_i}{p_i}\right)$ are considered.

Directing attention back to entropy, for $g(u) = -\log(u)$, a concave function with $g(1) = 0$, note the equality with taking the expectation of g with respect to a distribution and entropy, $E_{\mathbf{p}}[g(\mathbf{p}(x))] = H(\mathbf{p})$, and the divergence is the KL divergence, $D_{KL}(\mathbf{p}||\mathbf{q}) = \sum p_i \log\left(\frac{p_i}{q_i}\right)$. The Legendre dual of g , the dual of points and lines, is $f(u) = u \log(u)$ and the divergence has a ‘dual’ equality with KL divergence, $D_f(\mathbf{p}||\mathbf{q}) = -D_{KL}(\mathbf{p}||\mathbf{q})$. More importantly, this divergence coincides with the divergence derived from a cumulant generating function, which has the general form $\psi(\theta) = \log\left(\int \exp(\theta \cdot x) \exp(k(x)) dx\right)$, for some parameter θ and function k .

Therefore, mapping a point-cloud to Δ^d yields a rich structure one may exploit to extract information about the data.

B. Overview of Category Theory

Category theory generalizes mathematical structure through the collection objects and morphisms between objects, as well as their relationships with other objects and morphisms. Given the simplicity of the focus just on maps, the axiom structure is minimal.

A *category* is a collection of related objects, morphisms between objects, and an operation of morphisms denoted as the composition. These collection of objects and morphism is too broad and more structure is required. We require that the diagram in Equation 8 commutes. Furthermore, associativity of composition of morphisms holds. Hence, for morphisms f, g, h where the composition exists, $h \circ (g \circ f) = (h \circ g) \circ f$.

$$\begin{array}{ccc}
 X & \xrightarrow{f} & Y \\
 & \searrow^{g \circ f} & \downarrow g \\
 & & Z
 \end{array} \tag{8}$$

For a few illuminating examples, envisage the following. The category of groups (**Grp**) has objects that are the groups and the morphisms are homomorphisms, the category of sets (**Set**) whose objects are sets and the morphisms are the total functions, and the category of finite-dimensional vector spaces (**FinVec**) with objects the vector spaces over a field \mathbb{K} with finite number of basis vectors and morphisms the linear maps.

Given the collection of like objects and morphisms, one might ask the question how strong a relationship is there between two categories, typically chosen out of interest of analysis. Without changing the structure, a map between categories is introduced that takes objects to objects and morphisms to morphisms; this map is denoted as a **functor**. For a functor F and categories C and D where $F : C \rightarrow D$ where the following holds:

- for every object X in C , $F(X)$ is an object in D ;
- for a morphism f in C where $f : X \rightarrow Y$ then $F(f) : F(X) \rightarrow F(Y)$;
- for the identity function on X , id_X , $F(\text{id}_X) = \text{id}_{F(X)}$;
- and for morphisms f and g in C where $f : X \rightarrow Y$ and $g : Y \rightarrow Z$ then $F(f \circ g) = F(f) \circ F(g)$.

A simple example is the functor between the categories Grp and Set that ‘forgets’ the group structure and maps the elements in a group to just a set, and homomorphisms to morphisms that maps elements to elements.

Of course, the selection of a functor has the potential to be biased. Further keeping the structure in tacked, define a **natural transformation** as a map from functor to functor, ergo, $\eta : F \rightarrow F'$ for $F, F' : C \rightarrow D$, where

for objects in C are mapped to one another, and the compositions are commutative. That is, for object X , $\eta_X : F(X) \rightarrow F'(X)$ and for morphism in C , $f : X \rightarrow Y$, $\eta_Y \circ F(f) = F'(f) \circ \eta_X$. Thus, the diagram in Equation 9 commutes.

$$\begin{array}{ccc}
 F(X) & \xrightarrow{\eta_X} & F'(X) \\
 F(f) \downarrow & & \downarrow F'(f) \\
 F(Y) & \xrightarrow{\eta_Y} & F'(Y)
 \end{array} \tag{9}$$

This is only the surface of definitions and results from category theory and for in-depth explanations, examples, and essential characteristics, see [26–28]. In this manuscript, the category theoretical techniques applied are not too complex and the introduction maybe sufficient.

C. Pseudo-Entropy

For a basis of our definition of the entropy of special unitary operators, we briefly described von Neumann entropy. Using the concept of entropy to quantum states, von Neumann is defined to calculate the entropy of a density operator, say $\mathcal{A} = \sum p_i |i\rangle \langle i|$, where p_i ’s are the ‘frequency’ weights for the basis quantum states $|i\rangle$. With this operator, von Neumann entropy [29] is defined as $S(\mathcal{A}) := -\text{Tr}[\mathcal{A} \log(\mathcal{A})] = \sum_i p_i \log(p_i)$, hence the eigenvalues of the density matrix.

As previously discussed, quantum feature maps are variational schemes where real-world data points are taken as variables of the selected special unitary operators. Recall that a special unitary operator U has the decomposition $U = V\Lambda V^\dagger$ where V is unitary and Λ is a diagonal matrix, and the entries of Λ are the eigenvalues of the operator. The decomposition is a consequence of the Spectral Theorem [30], and this spectral decomposition is just a special case of singular value decomposition.

Since the eigenvalues are the ‘energy’ of the collection of quantum gates, with this decomposition, we apply von Neumann entropy to the diagonal matrix Λ . Hence, we define the function

$$S(U) = -\text{Tr}(\Lambda \log(\Lambda)). \tag{10}$$

Thus, the definition of pseudo-entropy only extends the domain of arguments fed into the von Neumann entropy function.

The definition of pseudo-entropy defined in Equation 10 is quite natural as one may see that

$$\begin{aligned}
 -\text{Tr}(U \log(U)) &= -\text{Tr}(V\Lambda V^\dagger \log(V\Lambda V^\dagger)) \\
 &= -\text{Tr}(V\Lambda V^\dagger V \log(\Lambda) V^\dagger) = \text{Tr}(V\Lambda \log(\Lambda) V^\dagger) \\
 &= -\text{Tr}(\Lambda \log(\Lambda) V^\dagger V) = \text{Tr}(\Lambda \log(\Lambda)).
 \end{aligned} \tag{11}$$

Moreover, since U is special unitary the eigenvalues are of the form $e^{\alpha i}$ for some $\alpha \in (-\pi, \pi)$, which yields

$$\begin{aligned} -\text{Tr}(\Lambda \log(\Lambda)) &= -\sum_j e^{\alpha_j i} \log(e^{\alpha_j i}) \\ &= -\sum_j (\cos(\alpha_j) + i \sin(\alpha_j)) \cdot (\alpha_j i) \\ &= -i \sum_j \alpha_j \cdot \cos(\alpha_j) + \sum_j \alpha_j \cdot \sin(\alpha_j). \end{aligned} \quad (12)$$

Consequently, $-\text{Tr}(\Lambda \log(\Lambda)) \in \mathbb{R}$ if and only if $\sum_j \alpha_j \cdot \cos(\alpha_j) = 0$.

Given that, essentially, the complex unit circle is the domain of this entropy function, one may this is the complex analytic extension of von Neumann entropy, which usually is the entropy for positive density operators. Since the complex unit circle crosses over any pre-selected branch-cut, for this definition we choose the standard branch cut for the complex logarithm, which is the negative real axis. Hence, the principal branch is $(-\pi, \pi)$ [22]. This branch is exactly the branch of the logarithm of matrix method in SciPy [31], which is essential for experiments described below.

Observe that, as was briefly noted, pseudo-entropy in this context gives the energy of the operator. Ergo, a zero value would be an operator that does not have the potential to manipulate the state of the qubit, which is just the identity operator; one may verify that the entropy of the identity operator is indeed zero. Furthermore, observe that complex pseudo-entropy values indicate entanglement, just as in the original derivation of pseudo-entropy. To understand why this is the case, Proposition 13 shows that circuits with only single qubit operators yield only positive real pseudo-entropy values.

Proposition 13. *If U represents the unitary operator of a circuit with only single qubit operators and -1 is not an eigenvalue then $S_{vN}(U) \in \mathbb{R}_{\geq 0}$. Furthermore, for general special unitary operators U_1 and U_2 , if -1 is not an eigenvalue for either operator and the addition of the exponents of eigenvalues from U_1 and U_2 do not cross over the principal branch then*

$$S_{vN}(U_1 \otimes U_2) = \text{Tr}(U_2) \cdot S_{vN}(U_1) + \text{Tr}(U_1) \cdot S_{vN}(U_2). \quad (14)$$

Proof. For a circuit with a single wire, ergo U is a 2×2 special unitary operator, observe that the eigenvalues of U are complex conjugates. Thus $S_{vN}(U) \in \mathbb{R}_{\geq 0}$. For $U = \bigotimes_i U_i$ the special unitary operator of a circuit with an arbitrary, but finite, number of wires, note that, for the spectral decomposition $U_i = V_i \Lambda_i V_i^\dagger$,

$$S_{vN}\left(\bigotimes_i U_i\right) = S_{vN}\left(\bigotimes_i \Lambda_i\right). \quad (15)$$

We claim that given an eigenvalue of U then the complex conjugate of this eigenvalue is also an eigenvalue of U . By Equation 15, we will focus on the diagonal matrix of eigenvalues. Observe that the eigenvalues of $U_1 \otimes U_2$ are

$$\begin{aligned} \Lambda_1 \otimes \Lambda_2 &= \begin{bmatrix} e^{i\theta_1} & 0 \\ 0 & e^{-i\theta_1} \end{bmatrix} \otimes \begin{bmatrix} e^{i\theta_2} & 0 \\ 0 & e^{-i\theta_2} \end{bmatrix} \\ &= \begin{bmatrix} e^{i\theta_1} e^{i\theta_2} & 0 & 0 & 0 \\ 0 & e^{i\theta_1} e^{-i\theta_2} & 0 & 0 \\ 0 & 0 & e^{-i\theta_1} e^{i\theta_2} & 0 \\ 0 & 0 & 0 & e^{-i\theta_1} e^{-i\theta_2} \end{bmatrix}, \end{aligned}$$

which clearly holds the claim. Induction finishes the claim. Therefore, $S_{vN}(U) \in \mathbb{R}_{\geq 0}$ for a general circuit with single qubit operators, since for $A_1, \dots, A_n \in \text{SU}(2)$ there exists a $C \in \text{SU}(2)$ where $A_1 \dots A_n = C$.

From Equation 15, with the decomposition $U_1 = V_1 \Lambda_1 V_1^\dagger$ and $U_2 = V_2 \Lambda_2 V_2^\dagger$, we have the equality $\text{Tr}(U_1 \otimes U_2 \log(U_1 \otimes U_2)) = \text{Tr}(\Lambda_1 \otimes \Lambda_2 \log(\Lambda_1 \otimes \Lambda_2))$. Considering the logarithm term we see that $\log(\Lambda_1 \otimes \Lambda_2) = \log(\Lambda_1 \otimes I \times I \otimes \Lambda_2) = \log(\Lambda_1 \otimes I) + \log(I \otimes \Lambda_2)$, since the matrices commute. Now, since the matrices are diagonal, $\log(\Lambda_1 \otimes I) = \log(\Lambda_1) \otimes I$ and $\log(I \otimes \Lambda_2) = I \otimes \log(\Lambda_2)$. The rest now follows. \square

Given that pseudo-entropy values are, in general, complex, Proposition 13 precisely shows that when entanglement is not introduced into a circuit there will never be imaginary or complex pseudo-entropy values.

The author independently derived the pseudo-entropy function from the work and definition in Nakata et al. [32]. In fact, pseudo-entropy defined in this manuscript is a particular case of holographic pseudo entropy. Nakata et al. [32] give a holistic explanation of pseudo-entropy and general view of entropy in quantum.

Moreover, the concept of pseudo-entropy are all just variations of von Neumann entropy applied to operators of different states [33–36]. Particularly, von Neumann entropy is applied to reduced transition matrix between two pure quantum states to gauge entanglement [32, 36, 37], and the continuous time states change in von Neumann entropy [34]. While the definition of pseudo-entropy differs from the idea in previous literature, given the only change is the domain of operators, the name of the entropy calculated should not change.

IV. CATEGORY THEORY AND THE FLOW OF INFORMATION

Before we delve into the derivation of the technique, consider the potential comparison of the entropy of the data and the expected state of a quantum feature map. At first glance, this appears to be the proper perspective, especially since this is the view among many papers on quantum machine learning. With this perspective, the

amplitude encoding scheme would be a perfect fit as each data point is mapped to a point on the simplex via a diffeomorphic function. However, Gennaro, Vlastic, and Pham [38] empirically displayed that this feature map trained statistical models that performed poorly.

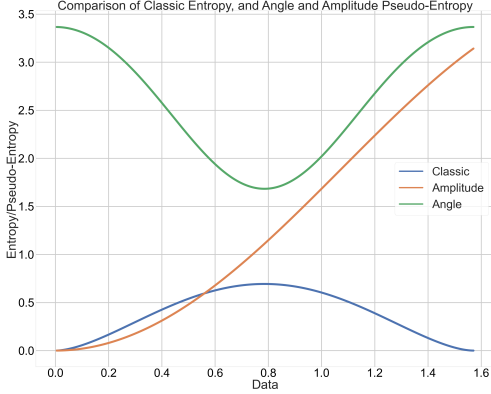


FIG. 3: Pseudo-entropy for the three different encodings of the unit circle: classical encoding (blue), amplitude encoding (green), and angle encoding (orange).

Throughout the manuscript, denote S_{Sh} as **classical entropy** and S_{vN} as **pseudo-entropy**.

A. Examples

For a simple example take the interval $[0, \pi/2]$ as the manifold that contains data points of a point-cloud. With this interval we calculate the Shannon entropy of each data point and the respective pseudo-entropy of the angle and amplitude feature maps.

In general, take $\theta \in (-\pi, \pi)$. Given such an angle θ , we set p_θ to be the probability distribution on the set $\{0, 1\}$ given by $p_\theta(0) = \cos^2(\theta)$ and $1 - p_\theta(1) = \sin^2(\theta)$. For this example, we call this assignment the *classical encoding* of each point θ on the unit circle with a state (probability distribution) p_θ on $\{0, 1\}$. Ergo, a function $p : S^1 \rightarrow \mathcal{P}(\{0, 1\})$, where $\mathcal{P}(X)$ denotes the set of probability distributions on a finite set X . We can also view $\mathcal{P}(\{0, 1\})$ as a convex subspace of $\mathbb{C}^{\{0,1\}}$, where \mathbb{C}^X denotes the algebra of complex-valued functions on a finite set X . Therefore, the encoding can be viewed as an embedding $p : S^1 \rightarrow \mathbb{C}^{\{0,1\}}$.

The angle and amplitude feature maps are explicitly described. For $\theta \in (-\pi, \pi)$, observe the well-known equality

$$R_X(\theta) = \exp\left(-i\frac{\theta}{2}X\right) = \begin{bmatrix} \cos(\theta/2) & -i\sin(\theta/2) \\ -i\sin(\theta/2) & \cos(\theta/2) \end{bmatrix}.$$

Now, given the restriction of θ , we take the map $\beta : S^1 \rightarrow \text{SU}(2) \otimes \text{SU}(2)$ sending θ to $\beta(\theta) := R_X(2\cos^2(\theta)) \otimes R_X(2\sin^2(\theta))$. This is precisely the *angle* encoding

scheme. Notice that the state created from the angle feature map is described in the mapping

$$R_X(2\cos^2(\theta)) \otimes R_X(2\sin^2(\theta)) |0\rangle^{\otimes 2} \in \mathbb{C}^2 \otimes \mathbb{C}^2.$$

The *amplitude* encoding scheme for θ is the map $\alpha : S^1 \rightarrow \text{SU}(2)$ sending θ to $\alpha(\theta) = R_X(2\theta)$. The encoded state is then $R_X(2\theta)|0\rangle \in \mathbb{C}^2$. The general amplitude encoding scheme is fairly intricate and is described in Section II A.

For the classical encoding the entropy and is given by the standard entropy of the probability distribution, namely

$$S_{Sh}(p_\theta) = -\cos^2(\theta) \log(\cos^2(\theta)) - \sin^2(\theta) \log(\sin^2(\theta)).$$

To compute the pseudo-entropy values of the amplitude and angle encoding operators, we may analytically describe their eigenvalues. The eigenvalues of α_θ are $\{e^{i\theta}, e^{-i\theta}\}$. Therefore, the pseudo-entropy of the amplitude encoding operator is

$$\begin{aligned} S_{vN}(\alpha(\theta)) &= -e^{i\theta} \log(e^{i\theta}) - e^{-i\theta} \log(e^{-i\theta}) \\ &= -e^{i\theta}(i\theta) - e^{-i\theta}(-i\theta) \\ &= 2\theta \sin(\theta). \end{aligned}$$

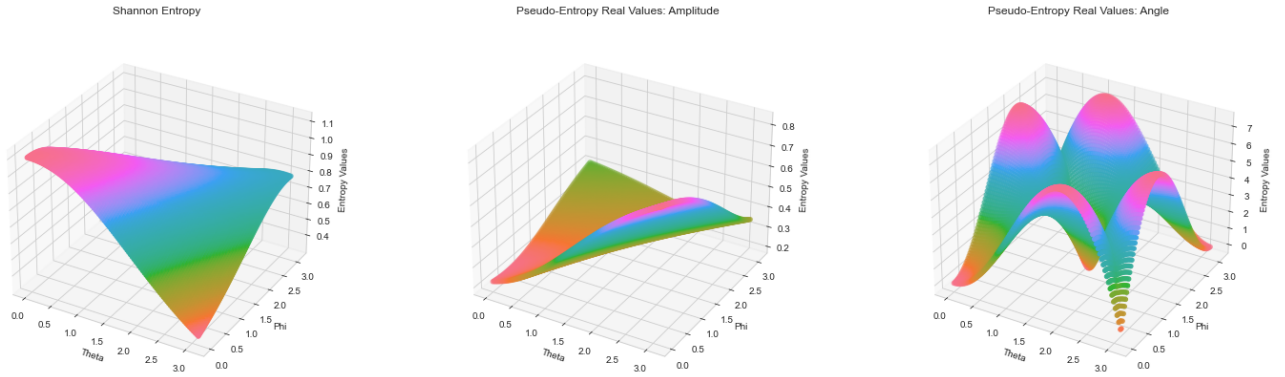
Finally, the eigenvalues of β_θ are $\{e^{i\cos(2\theta)}, e^{-i\cos(2\theta)}, e^i, e^{-i}\}$. Hence, the pseudo-entropy of the angle encoding operator is

$$\begin{aligned} S_{vN}(\beta(\theta)) &= -e^{i\cos(2\theta)} \log(e^{i\cos(2\theta)}) - e^i \log(e^i) \\ &\quad - e^{-i\cos(2\theta)} \log(e^{-i\cos(2\theta)}) - e^{-i} \log(e^{-i}) \\ &= e^{i\cos(2\theta)}(i\cos(2\theta)) - e^{-i\cos(2\theta)}(-i\cos(2\theta)) \\ &\quad - e^i(i) - e^{-i}(-i) \\ &= 2\cos(2\theta) \sin(\cos(2\theta)) + 2\sin(1). \end{aligned}$$

We plot the pseudo-entropy values to compare them visually in Figure 3. Observe the entropy of amplitude encoding steadily increases, while it appears that that entropy angle encoding and data are anticorrelated. In fact, these entropies have a Pearson correlation statistic [39] of -0.985 . Moreover, observe the tremendous difference in domains to calculate pseudo-entropy and entropy of a data point. Thus, it is not possible to apply standard information theoretic techniques, such as KL divergence and mutual information.

The reduced interval example, while illuminating, is fairly restrictive. We expand to the space $[0, \pi]^2$ and take the general feature maps of angle, amplitude, and IQP. For each pair of data points, these points are mapped directly into the angle and IQP encoding schemes. For Shannon entropy, each pair of data points are mapped to the simplex through the diffeomorphism in Equation 17. This point in the simplex also fed into the amplitude feature map. The subtleties of the diffeomorphism are discussed in Section IV B.

Shannon entropy and pseudo-entropy for the angle and amplitude feature maps are given in Figure 4. Interestingly, the angle feature map came into computational



(a) Shannon entropy of the data points in $[0, \pi]^2$ mapped to the simplex.

(b) Pseudo-entropy of the amplitude encoding scheme.

(c) Pseudo-entropy of the angle encoding scheme.

FIG. 4: Entropy comparison for the data lying in $[0, \pi]^2$ and respective encoding schemes. For Shannon entropy, the data points are mapped to the simplex via the map in Equation 17.

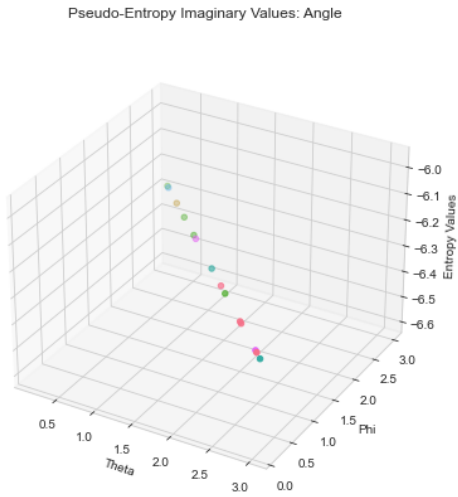


FIG. 5: Discontinuous points of the pseudo-entropy angle encoding of the space $[0, \pi]^2$.

issues with the branch cut, essentially with the pairs of identical angles; these discontinuous points are given in Figure 5.

Lastly, the pseudo-entropy for the IQP feature map is given in Figure 6. The values are separated into real values and imaginary values. A small ball around the point $(0, 0)$ displayed calculation errors and was taken out to mitigate any confusion from analyzing the graphs of the entropy values.

B. Categorical Derivation of Feature Maps and Pseudo-Entropy

The square of maps in Equation 16, which may not necessarily commute, shows the flow of a data point in the point-cloud, where we recall that S_{Sh} is Shannon entropy and S_{vN} is pseudo-entropy, f is a diffeomorphism, and U is a quantum feature map.

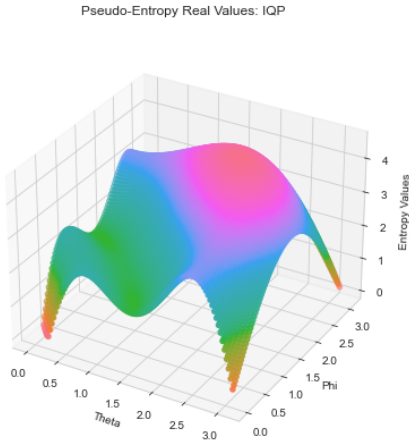
$$\begin{array}{ccc}
 M_n & \xrightarrow{f} & \Delta^{n+1} \\
 U \downarrow & & \downarrow S_{Sh} \\
 \text{SU}(2^m) & \xrightarrow{S_{vN}} & \mathbb{C}
 \end{array}$$

(16)

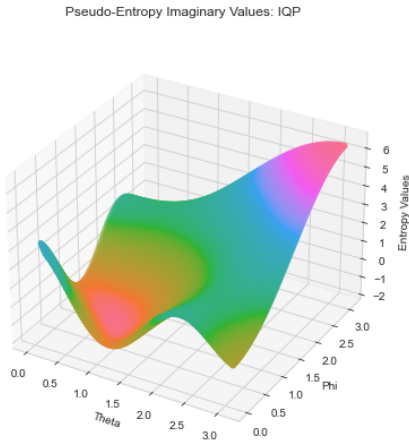
We posit that if the square of maps commutes then the U retains information with respect to entropy. However, the square as given is too simple for analysis as the points that mapped from entropy and points mapped from pseudo-entropy have very little overlapping codomains. Adjusting for the simple space of scalars \mathbb{C} , we will consider the function graphs $G(M, S_{Sh} \circ f) = \{(x, S_{Sh} \circ f(x)) | x \in M\}$ and $G(M, S_{vN} \circ U) = \{(x, S_{vN} \circ U(x)) | x \in M\}$ as the final codomain of the square of arrows; in general, denote $G(M, f) := \{(x, f(x)) \forall x \in M\}$ as the graph of a function.

With the expanded codomain in the bottom right in Equation 16 to the function graph, this square may be described with the following categories, which are fully described further in the section:

- category of real valued embedded manifolds, EmbedMan;
- category of special unitary operators, Feat ;



(a) Real values of the Pseudo-entropy of the IQP encoding scheme.



(b) Imaginary values of the Pseudo-entropy of the IQP encoding scheme.

FIG. 6: Pseudo-entropy for the IQP feature map on the space $[0, \pi]^2$, excluding a small ball around the point $(0, 0)$.

- and category of embedded subspaces $M \subseteq \mathbb{R}^n \times \mathbb{C}$, $\text{EmbedMan}^{\mathbb{C}}$.

Notice that there are many options for the morphism f , but many of these options change the values of, at least one, column of the data, changing the structure. Since the graph $G(M, S_{Sh} \circ f)$ needs to be simple to retain information, we will only apply the parameter-less function

$$E(x) := \frac{1}{e^{x_1} + \dots + e^{x_d} + e^0} (e^{x_1}, \dots, e^{x_d}, e^0), \quad (17)$$

where, since E maps points to the interior of the simplex,

$$E^{-1}(x) = \left(\log\left(\frac{p_1}{p_{d+1}}\right), \dots, \log\left(\frac{p_d}{p_{d+1}}\right) \right). \quad (18)$$

For the function E , one may show that as one of the entries in the data point $x_i \rightarrow \pm\infty$ then $E(x)$ approaches the face, or an embedded face, of the n -simplex.

Observe that E is a simple form of a Gibbs measure [40]. Particularly, $x \rightarrow (x_1, \dots, x_d, 0)$, thus, $M \times \{0\}$, then for $i \in \{1, 2, \dots, d+1\}$ for a created random variable, say X , $P(X = i) = \frac{e^{x_i}}{\sum_{j=1}^{d+1} e^{x_j}}$. This is precisely the i^{th} entry in the vector $(x_1, \dots, x_d, 0)$.

In general, a Gibbs measure is of the form $P(X = x) = \frac{e^{-\beta H(x)}}{\sum_{x_i} e^{-\beta H(x_i)}}$, for an energy function H . However, for $H_\beta := -\beta H$, this is just the map $E \circ H_\beta$. Therefore, the function H_β deforms the original manifold, which adds unnecessary extra structure to the diffeomorphism E .

Furthermore, we claim that E is unique up to composition. Therefore, as noted above, the addition of composition adds unnecessary structure to the diffeomorphism, complicating the analysis. Thus, E will be applied without other morphisms.

Claim 19. *The diffeomorphism defined in Equation 17 is unique up to composition.*

Proof. Take g as an arbitrary diffeomorphism where $g : \mathbb{R}^n \rightarrow \Delta^{d+1}$ for some arbitrary $d \in \mathbb{N}$. Then the map $E^{-1} \circ g : \mathbb{R}^d \rightarrow \mathbb{R}^d$ is a diffeomorphism. Denote $\hat{x} = E^{-1} \circ g(x)$ for all $x \in \mathbb{R}^d$. Applying Equation 18 yields the equality $g(x) = g(x)_{d+1} \cdot (e^{\hat{x}_1}, \dots, e^{\hat{x}_d}, 1)$. Therefore, g is equal to E with compositions. \square

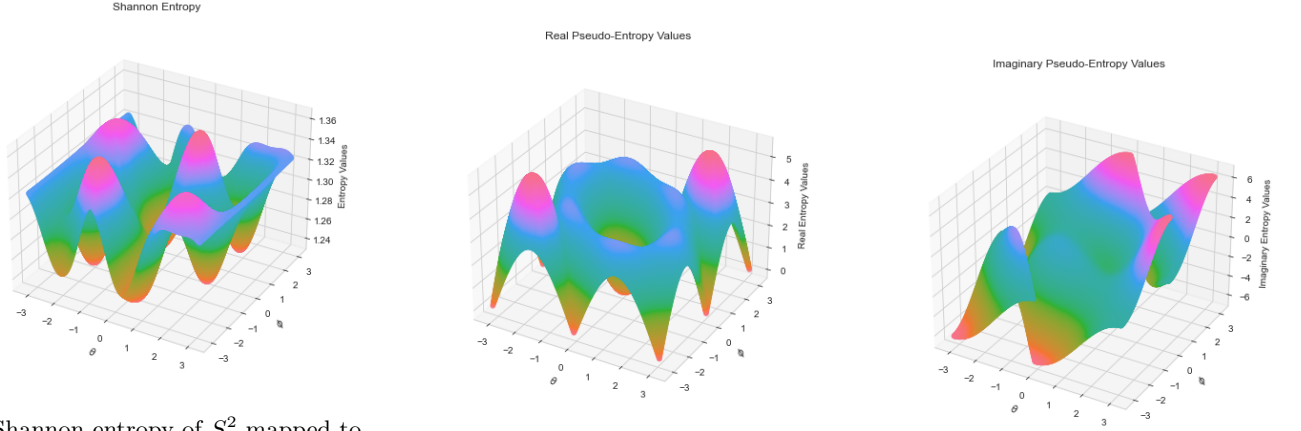
Observe that the proof is not unique for the map E since it uses the characteristics of diffeomorphisms. However, the property in Claim 19 coupled with the connection to a Gibbs measure yields a physical intuition into the technique.

The category EmbedMan consists of embedded manifolds M within a Euclidean space, ergo, $M \subseteq \mathbb{R}^n$ for some $n \in \mathbb{N}$. For for $N \subseteq \mathbb{R}^{n'}$, a morphism from M to N is a smooth map $\rho : \mathbb{R}^n \rightarrow \mathbb{R}^{n'}$ with $\rho(M) \subseteq N$.

The category $\text{EmbedMan}^{\mathbb{C}}$ is described similarly as EmbedMan , with the distinction that all manifolds are embedded as $M \subseteq \mathbb{R}^n \times \mathbb{C}$ and morphisms are not necessarily smooth and potentially not continuous.

The Feat category objects are tuples (M, U) where M is an embedded manifold and U is a quantum feature map where $U = U|_{\mathbb{R}^n} : M \rightarrow \text{SU}(2^{m_n})$ and the exponential m_n is contingent on the dimension of the embedded manifold. Morphisms in this category are subtle, where, intuitively, the morphism is a smooth map between embedded manifolds, but the quantum feature map is interchangeable. Particularly, for a morphism g_{UV} between objects (M, U) and (N, V) , U is replaced with V and $g_{UV}|_M$ is a smooth map from \mathbb{R}^n to $\mathbb{R}^{n'}$ where $g_{UV}|_M(M) \subseteq N$, which is a morphism in EmbedMan . The Feat category was crafted so filter for particular quantum feature maps.

Collecting all of this information culminates to the triangle in Equation 20, which may not necessarily com-



(a) Shannon entropy of S^2 mapped to the simplex with the E map. Given the dimensions, entropy values are given with respect to the angles.

(b) Real values of the pseudo-entropy where θ and ϕ are the angle of the points on S^2 .

(c) Imaginary values of the von Neumann entropy.

FIG. 7: Entropy for the S^2 manifold.

mute.

$$\begin{array}{ccc}
 & \text{EmbedMan} & \\
 & \swarrow U & \searrow S_{vN} \\
 \text{Feat} & \xrightarrow{S_{Sh}^E} & \text{EmbedMan}^{\mathbb{C}}
 \end{array} \quad (20)$$

The map U , with some abuse of the notation, is a mapping with the quantum feature map U that is fairly intuitive where objects $U(M) = (M, U)$ and morphisms $U(g) = g_U^U$. Hence, U is the only quantum feature map which keeps embedded manifolds from the EmbedMan category essentially fixed. Given the structure of the EmbedMan category, one may see that U holds the properties of a functor.

Using the construction of the categories and description of the general entropy mapping, both S_{Sh}^E and S_{vN} map objects, the embedded manifolds, to another embedded manifold via the function graph. Morphisms under these two maps take the original morphism and extends them with the function graph G , where for $g : M \rightarrow N$ we have $S_{Sh}^E(g) : G(M, S_{Sh}^E) \rightarrow G(N, S_{Sh}^E)$ with codomain $G(g(M), S_{Sh}^E)$, and for the morphism $g_{U'V} : (M, U') \rightarrow (N, V)$ is transformed with $S_{vN}(g_{U'V}) : G(M, S_{vN} \circ U') \rightarrow G(N, S_{vN} \circ V)$. Again, with the codomain $G(g(M), S_{vN} \circ V)$. From the tuple, since the quantum feature map is interchangeable, but the domain is mapped with a morphism from the EmbedMan category, one may observe the morphisms commute if the mappings between the embedded manifolds commute. With this observation one may see that S_{Sh}^E and S_{vN} are functors.

Continuous morphisms between objects mapped from the two functors raises the question that the composed functor $S_{vN} \circ U$ may map manifolds to unconnected

subspaces. Claim 21 shows that the extended pseudo-entropy applied to a fixed quantum feature map is a continuous function, but with the branch of $\theta \in (-i\pi, i\pi)$ for the eigenvalues e^θ . Ergo, the branch cut is necessary to ensure continuity, and for applications, a quantum feature map is assumed to not have an eigenvalue of -1 , as previously discussed. Given the number of rotations in an arbitrary encoding scheme, this assumption is not very restrictive. Figure 8 displays the importance incorporating the branch, emphasizing, one must be cautious.

We now show that eigenvalues are continuous with respect to the parameter, ergo, the data points.

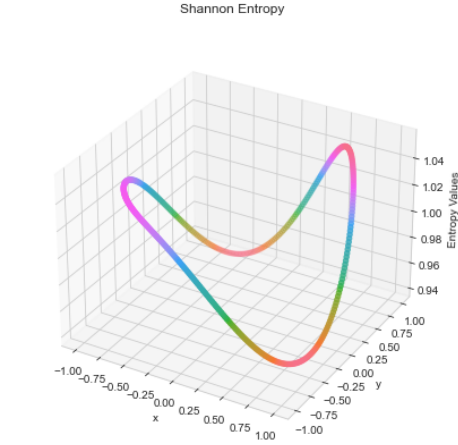
Claim 21. *With an arbitrary eigenvalue of an arbitrary quantum feature map, the eigenvalue is continuous with the respective parameter(s).*

Proof. Since the general form of a quantum feature map is $(\theta_1, \dots, \theta_n) \rightarrow \bigotimes_{i=1}^n U_i(\theta_i)$, where $U_i(\cdot)$ is a special unitary operator. Each operator U_i is arbitrarily given, which makes the operator difficult to analyze. However, by the Cartan decomposition [41], without loss of generality we may assume $U_i \in \text{SU}(2)$ for all variational operators; non-variational operators, like the CNOT gate, have fixed eigenvalues, which does not have a constant affect on the final eigenvalues. Observe that the general operator in $\text{SU}(2)$ is of the form $\begin{bmatrix} \cos(\frac{\gamma}{2}) & -e^{i\lambda} \sin(\frac{\gamma}{2}) \\ e^{i\phi} \sin(\frac{\gamma}{2}) & e^{i(\phi+\lambda)} \cos(\frac{\gamma}{2}) \end{bmatrix}$, with the eigenvalues of

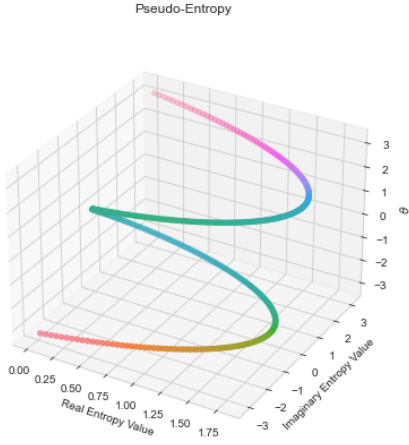
$$\frac{(1 + e^{i(\phi+\lambda)}) \cos(\frac{\gamma}{2}) \pm \sqrt{(1 + e^{i(\phi+\lambda)})^2 \cos^2(\frac{\gamma}{2}) - 4e^{i(\phi+\lambda)}}}{2},$$

which is continuous for any combinations of the parameters.

For eigenvectors of a matrix that is a tensor product, recall that for matrices A and B with eigenvectors and



(a) Shannon entropy of S^1 mapped to the simplex with the E map.



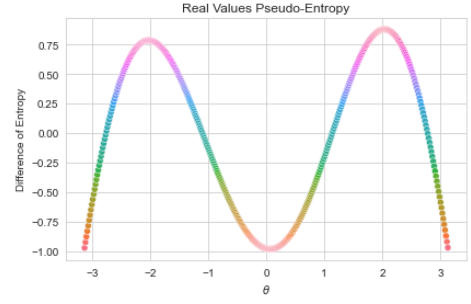
(b) The pseudo-entropy where θ is the angle of the points on S^1 , but $\theta \in (-\pi, \pi)$.

FIG. 8: Entropy comparison of data points taken from S^1 .

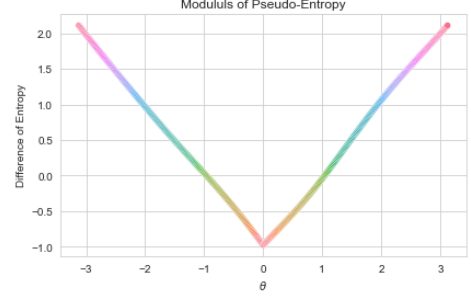
eigenvalues $a|a\rangle$ and $b|b\rangle$ then for $U = A \otimes B$ the vector $|a\rangle \otimes |b\rangle$ is an eigenvector with eigenvalue ab . For a tensor product of more than two matrices, from the properties of the tensor it is clear one may recursive find eigenvectors and eigenvalues. To address the possibility of degenerate eigenvectors, (eigenvectors that are not the tensor product of eigenvectors), notice that for a special unitary matrix of size $n \times n$ there are n orthogonal eigenvectors, the tensor product of all possible combinations of the eigenvectors of each U_i within tensor product of $\otimes_{i=1}^n U_i(\theta_i)$, say of size $2^n \times 2^n$, is equal to 2^n , there can be no other possible eigenvectors.

Therefore, since the product of continuous functions is continuous, the claim is finished. \square

With all of this information one has to ask of the existence of a functor V that ensures the triangle in Equation



(a) For S^1 , this is the difference of the real value of the pseudo-entropy and Shannon entropy.



(b) For S^1 , this is the difference of the modulus of the pseudo-entropy and Shannon entropy.

FIG. 9: These figures display a pattern between the entropies.

20 commute. Commuting implies that for all objects, $(M, S_{Sh}^E(M)) = (M, S_{vN} \circ V(M))$, ergo, for all $x \in M$ we have $S_{Sh}^E(x) = S_{vN} \circ V(x)$. However, given the definition of S_{vN} and the values of the eigenvalues, it is clear that in general $S_{Sh}^E(x) \neq S_{vN} \circ V(x)$. Thus, outside of the trivial case when both entropy values are zero, it is not possible for this map to commute.

While there does not exist a functor U for the triangle to commute, one has to ask the existence of the general condition of a fixed morphism l such that $S_{Sh}^E = l \circ S_{vN} \circ U$. Ergo, the triangle in Equation 20 commutes. Note that the map from pseudo-entropy to Shannon entropy is an easier case since l starts from a high dimensional space and maps to a lower dimensional space, $l : \mathbb{C} \rightarrow \mathbb{R}_{\geq 0}$.

However, before we delve into answering this question, observe that the two functors are isomorphic, ergo, there exists natural transformation between them. For the construction of a natural transformation, define a map η from $l \circ S_{vN} \circ U$ to S_{Sh}^E where for a smooth embedded manifold M and $c \in [0, 1]$ we construct the function graph

$$\begin{aligned} & G(M, (1-c) \cdot l \circ S_{vN} \circ U + c \cdot S_{Sh}^E) \\ &= \left\{ \left(x, (1-c) \cdot l \circ S_{vN} \circ U(x) + c \cdot S_{Sh}^E(x) \right) \mid x \in M \right\}. \end{aligned}$$

With this construction, $c = 0$ corresponds to $l \circ S_{vN} \circ U$ and $c = 1$ corresponds to S_{Sh}^E . For the trivial 2-

category, $\mathbf{2} = \{0 \rightarrow 1\}$, consider the Cartesian category $\text{EmbedMan} \times \mathbf{2}$. Then it is clear that for the morphism and objects $g : M \rightarrow N$ in EmbedMan , the diagram below commutes.

$$\begin{array}{ccc}
 (M, 0) & \xrightarrow{(g, \mathbf{1}_0)} & (N, 0) \\
 \downarrow (\mathbf{1}_M, 0 \rightarrow 1) & & \downarrow (\mathbf{1}_N, 0 \rightarrow 1) \\
 (M, 1) & \xrightarrow{(g, \mathbf{1}_1)} & (N, 1)
 \end{array}
 \tag{22}$$

Thus, there exists a functor $\alpha : \text{EmbedMan} \times \mathbf{2} \rightarrow \text{EmbedMan}^{\mathbb{C}}$ where $\alpha(M, 0) = l \circ S_{vN} \circ U(M)$, $\alpha(M, 0 \rightarrow 1) = S_{Sh}^E(M)$, and $\alpha(M, 0 \rightarrow 1) : l \circ S_{vN} \circ U(M) \rightarrow S_{Sh}^E(M)$. Therefore, α is a natural transformation. One may see that this functor is the homotopy oriented derivation of a natural transformation, as discussed in [27, 28], where validity holds from the function graph mappings of the functors.

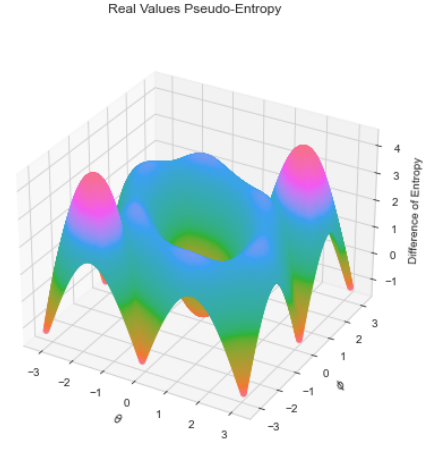
Now that the existence of a natural transformation has been established, we now ask about the existence of a global morphism where $l \circ S_{vN} \circ U \equiv S_{Sh}^E$. To display the difficulty, take the example of spheres S^1 and S^2 where, for the phase gate given by Equation 4 and the spheres converted to angles the feature map $(\theta_1, \dots, \theta_n) \mapsto \bigotimes_i p(\theta_i) |0\rangle^{\otimes n}$. For the Shannon entropy, the points on the sphere are mapped to the simplex via the map E . For S^1 , Figure 8 shows the Shannon entropy with respect to the data points and the pseudo-entropy with respect to the angle and the complex number is separated into pairs.

With the low-level domains of the real values of the pseudo-entropy and the modulus of the von Neumann entropy, taking the difference of each domain and Shannon entropy displays structure in both; Figure 9 shows a linear pattern and a periodic pattern, with some subtleties at certain intervals.

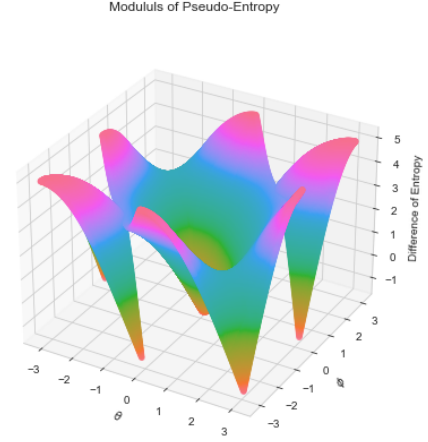
Moving the investigation to S^2 with the results shown in Figure 7, one would hope to see a scaled linear pattern or a scaled periodic pattern. However, while there appears to be a pattern in either case, these patterns do not follow the patterns found on the S^1 manifold, implying a more elaborate relationship between the entropy values. Interestingly, all of the patterns appear to be close to symmetric about the points 0 and $(0, 0)$, respectively.

C. Local Morphisms

The morphisms between the Shannon entropy and pseudo-entropy on S^1 and S^2 suggests the existence of a natural transformations with non-trivial maps. How-



(a) For S^2 , this is the difference of the real value of the pseudo-entropy and Shannon entropy.



(b) For S^2 , this is the difference of the modulus of the pseudo-entropy and Shannon entropy.

FIG. 10: These figures display an intricate pattern between the entropies.

ever, it also suggests that a scalable morphism l where $l \circ S_{vN} \circ U \equiv S_{Sh}^E$ does not exist. From this observation, take an arbitrary smooth embedded manifold M and an arbitrary $x \in M$, then l there is an f_M^l where $l(S_{vN}(U(x))) = f_M^l(S_{Sh}(x))$. Given the nature of the mappings of entropy and pseudo-entropy, one may see that f_M^l is 1-1, and therefore exists.

Furthermore, f_M^l maybe smooth and has a potential to be symmetric. For example, for two points $x_0 \neq x_1$ where $l(S_{vN}(U(x_0))) = l(S_{vN}(U(x_1)))$, a likely scenario emphasized by the permutation of entries of data points and displayed by previous examples, would imply $f(x_0) = f(x_1)$, and thus, for embedded manifolds with symmetric permutation f_M^l is a symmetric function.

Since $S_{sh}(\cdot)$ is continuous and, by Claim 21, $S_{vN}(U(\cdot))$ is continuous, then mapping a point $x \in M$ for both

maps, when it exists, is well-defined. Thus, there exists a function $f : \mathbb{R} \rightarrow \mathbb{R}$ such that, where $l \circ S_{vN} \circ U(x)$ is defined for all $x \in M$, we have $f(S_{Sh}(x)) = l(S_{vN}(U(x)))$, albeit, at least locally to the manifold and the function l . Furthermore, one may show that if l is continuous then f is also continuous.

We formally make the denotation of these functions and include the function graph in order to keep context of the values.

Definition 23. For an arbitrary quantum feature map, U , and arbitrary smooth manifold M , take $x \in M$ where $S_{vN} \circ U$ is defined. We call the map $l : (M, S_{vN}(U(M))) \rightarrow \mathbb{R}$ the translation of the pseudo-entropy, or just the *translation*. We call the map $f : (M, S_{Sh}(M)) \rightarrow \mathbb{R}$ where $f(x, S_{Sh}(x)) = l(S_{vN}(x, U(x)))$ the *fit*.

Given the difficulty of finding an analytic form of the fit function, we calculate Spearman rank correlation [39], and the nonlinear Xicor correlation [42]. The Xicor correlation coefficient has values in the interval $[0, 1]$, where zero indicates no relationship and one indicates a strong relationship. To give more context to the Xicor correlation coefficient, Spearman correlation coefficient, a generalization of the well-known Pearson correlation, tests the linear relation between two data sets and has values in $[-1, 1]$. Negative values indicate an inverse linear relationship, positive values a direct linear relationship, and values near zero indicate no relationship. For simplicity, throughout the analysis we take the translation function as either the function that takes the *real values* of pseudo-entropy or the *modulus* of pseudo-entropy.

1. Expressivity

Schuld, Sweke, and Meyer [4] derived a method to empirically test the expressivity of a quantum circuit by calculating the expectation value measurement, taking the partial Fourier series, and determining which complex function represents this expectation. Specifically, the authors analyze the function $f_\theta(x) = \langle 0|U^\dagger(x, \theta)\mathcal{M}U(x, \theta)|0\rangle$, where $U(x, \theta)$ is a variational operator with L -layers and potential repeated uploads of the data and \mathcal{M} is an observable. For simplicity, since θ is fixed, the term is dropped. The operator has the form $U(x) = W^{(L+1)}S(x)W^{(L)}S(x)\dots W^{(2)}S(x)W^{(1)}$, then, taking number of the layers, L , and number of wires in the circuit, say d , into consideration, we may rewrite the expectation function as $f(x) = \sum_{\mathbf{k}, \mathbf{j} \in [d]^L} e^{i(\Lambda_{\mathbf{k}} - \Lambda_{\mathbf{j}})x} a_{\mathbf{k}, \mathbf{j}}$. With

this notation, $[d]^L$ is the set of any L integers between $1, \dots, d$, $\Lambda_{\mathbf{j}} = \sum_{i=1}^L \lambda_{j_i}$, which is the sum of eigenvalues, and $a_{\mathbf{k}, \mathbf{j}} = \sum_{i, i'} (W^*)_{1k_1}^{(1)} (W^*)_{j_1 j_2}^{(2)} \dots (W^*)_{j_i i}^{(L+1)} \mathcal{M}_{i, i'} \times$

$W_{i' j_i}^{(L+1)} \dots W_{j_2 j_1}^{(2)} W_{j_1 1}^{(1)}$, which just the measurement of the variational layers.

Since the expectation function $f(x)$ is directly affected by the eigenvalues, which is quite natural and not at all surprising, it appears there is a relationship between expressivity and pseudo-entropy. Of course, since the circuit is measured and the function is the expected value, expressivity has a more intricate form than pseudo-entropy. However, while pseudo-entropy directly measures the energy of an operator, expressivity implicitly measures the energy through function representation. This implicit measuring gives a high score to the amplitude encoding scheme, yielding a potential for a circuit to create noise.

To illuminate the last statement, take the ‘warm-up application’ example in [4]. In this example the authors observe that, for a single qubit operator, a single rotation operator has a simple function representation, and repeated data-upload generates intricacy. For this example we consider the interval $(0, 2\pi)$ and the operators $H = \frac{1}{\sqrt{2}} \begin{bmatrix} 1 & 1 \\ 1 & -1 \end{bmatrix}$, which is the Hadamard gate, and $S = \begin{bmatrix} 1 & 0 \\ 0 & i \end{bmatrix}$ and $T = \begin{bmatrix} 1 & 0 \\ 0 & \exp(i\pi/4) \end{bmatrix}$, which are respective fixed values of the phase gate, where $\theta \in \{\pi/2, \pi/4\}$. Consider two operators,

$$HR_z(x)H \quad (24)$$

$$TR_y(x)T^\dagger \cdot SR_x(x)S^\dagger \cdot HR_z(x)H.$$

Table I shows that there is little difference between the operators in Equation 24. However, there is a noticeable increase in the linear relationship with the entropy of the data and the pseudo-entropy of the deeper circuit.

Correlations of Expressivity Example and Pseudo-Entropy			
Circuit	Function	Spearman	Xicor
HR_zH	Modulus	-.5182	.9806
$TR_yT^\dagger SR_xS^\dagger HR_zH$	Modulus	-.5772	.9805

TABLE I: For the operators in Equation 24, the Spearman and Xicor correlations are calculated between the entropy of the data and the pseudo-entropy of both circuits. The modulus of a complex number is taken as the function to map pseudo-entropy to the reals. When the real value from the pseudo-entropy is taken the correlations are exactly the same as the modulus, and so it was not included.

2. Symmetric Encoding

Symmetry with respect to reflection is perceived in Figure 9b and in Figure 9a in the example of S^1 and the phase gate encoding. Furthermore, one may see that the phase gate encoding is a representation of the abelian group action of rotations on the data set. Therefore,

keeping the symmetry around reflection structure of S^1 in tact.

The group representation observation from the simple example above is similar to the derivation of feature maps and symmetry in Meyer et al. [12]. However, Meyer et al. used the symmetric group representation capturing the symmetry of a data set to directly guide in crafting an encoding scheme. With a collection of (semi-)labeled points $\{(\mathbf{x}_i, y_i)\}_i$ and the representation of a symmetric group \mathcal{S} , say V_s , where for arbitrary \mathbf{x} and function of labels y , $y(V_s(\mathbf{x})) = y(\mathbf{x})$ for all $s \in \mathcal{S}$, a feature map U and some representation of \mathcal{S} , call it $U_s \in \text{SU}(2^n)$, must have the property $U(V_s(\mathbf{x})) = U_s U(\mathbf{x}) U_s^\dagger$ for all $s \in \mathcal{S}$.

One may see the phase gate feature map does not hold the equality $p(V_s(\theta)) = U_s P(\theta) U_s^\dagger$, for the group representation U_s for all $s \in \mathcal{S}$. Particularly, for a point on the circle, (x, y) the function $\text{atan2}(y, x)$ yields the angle $\theta \in (-\pi, \pi)$, and the negative of argument is a rotation of $\pm\pi$, which implies $e^{i\text{atan2}(y, -x)} = e^{i\text{atan2}(y, x)} e^{i\pi} = e^{i\text{atan2}(-y, x)}$; an analytic formula for $\text{atan2}(x, y)$ exists but is quite intricate. Working with just the rotation of negatives, there does not exist a $U \in \text{SU}(2)$ such that $p(\text{atan2}(y, -x)) = U p(\text{atan2}(y, x)) U^\dagger$.

Observe the quantum feature maps derived in Meyer et al. [12], using the logic in Equation 11, we have the equality

$$\text{Tr} \left(U(V_s(\mathbf{x})) \log \left(U(V_s(\mathbf{x})) \right) \right) = \text{Tr} \left(U(\mathbf{x}) \log \left(U(\mathbf{x}) \right) \right), \quad (25)$$

hence $S_{vN}(U(V_s(\mathbf{x}))) = S_{vN}(U(\mathbf{x}))$. Now, connecting Shannon entropy and pseudo-entropy, we take a continuous translation l , and, consequently, the respective fit function f is also continuous. Recall that for a fixed arbitrary $s \in \mathcal{S}$, the function V_s is linear and continuous. Ergo, for an arbitrarily small $\epsilon > 0$, for $x_0, x_1 \in M$ where $|\mathbf{x}_0 - \mathbf{x}_1| < \epsilon$ there exists a $\delta > 0$ such that $|f(S_{Sh}(\mathbf{x}_0)) - f(S_{Sh}(\mathbf{x}_1))| < \delta$, then, since $S_{vN}(U(x)) = S_{vN}(U(V_s(\mathbf{x}_1)))$, $|f(S_{Sh}(V_s(\mathbf{x}_0))) - f(S_{Sh}(V_s(\mathbf{x}_1)))| < \delta$. Since this inequality holds for all $s \in \mathcal{S}$, the fit function f is periodic, yielding a deeper relationship between the entropy and pseudo-entropy.

To summarize the argument, a periodic fit function indicates a strong relationship, and a symmetric encoding scheme with a continuous translation function yields a symmetric fit function. However, as there is potential for periodic fit functions outside of symmetric encoding, this technique generalizes the symmetric technique in Meyer et al. [12].

To finish this subsection, we address the observation in Meyer et al. [12] about the existence of more than one symmetric feature map and the importance of checking the expressibility of the schemes in the ‘Pit-falls to avoid’ subsection. Ergo, ansatz is not enough to determine a feature map to apply. To display this, consider the unit circle with angle values of $(-\pi, \pi)$. The symmetric rotations and reflections can be cap-

tured with the Klein’s four-group $\mathbb{Z}_2 \times \mathbb{Z}_2$. Following the example in [12], we take the representation of $V_{(1,0)} = \begin{bmatrix} 1 & 0 \\ 0 & 1 \end{bmatrix}$, $V_{(0,0)} = \begin{bmatrix} 0 & 1 \\ 1 & 0 \end{bmatrix}$, $V_{(0,1)} = \begin{bmatrix} -1 & 0 \\ 0 & -1 \end{bmatrix}$, and $V_{(1,1)} = \begin{bmatrix} 0 & -1 \\ -1 & 0 \end{bmatrix}$. Then for the encoding scheme $U_G(x_1, x_2) = G(x_1) \otimes G(x_2)$, where $G \in \{R_y, R_z\}$, one may calculate that $U_G(x_2, x_1) = \text{SWAP} U_G(x_1, x_2) \text{SWAP}$ and $U_G(-x_1, -x_2) = (X \otimes X) U_G(x_1, x_2) (X \otimes X)$. This begs the question as to which one of the two operators to use. Intuitively, it may not matter which scheme to apply since either operator creates a spin, albeit on their respective ‘axis’ on the Bloch sphere. Given the shortcoming of expressibility demonstrated in Section IV C 3, we will calculate the ‘goodness’ of the fit function for both encoding schemes. The respective Spearman and Xicor correlation coefficients for U_{R_z} is (.0020, .9613), and the correlation coefficients for U_{R_y} are (.0015, .9613), implying there is no significant difference between the feature maps, and thus the ansatz holds.

3. Expressibility

Sim, Johnson, and Aspuru-Guzik [2] derived a method to test the efficacy of a quantum feature map, denoted as **expressibility**. Expressibility refers to the ability of a circuit to generate the full range of pure states with respect to Hilbert space the quantum gates are acting on. For example, with a single qubit how well does a circuit capture states on the Bloch sphere. Particularly, for a given encoding technique, expressibility applies KL divergence, or symmetric KL divergence, to the Haar probability measure of the respective dimension of the data and the density of the states outputted from the feature map. Ergo, the score is inversely proportional to the expressibility of the feature map.

It is claimed that the concept of expressibility can be described through pseudo-entropy. To see this, consider the collection of eigenvalues and eigenvectors of a feature map with low expressibility, denoted as *low*, against a feature map with high expressibility, denoted as *high*. Low expressibility implies that the Haar probability measure of the states is concentrated around a few states, with the tail of this probability measure very small. Thus, there is a concentration of the collection of eigenvalues and vectors for a low feature map, leading to a concentration of pseudo-entropy values, indicating that the translation function is not smooth, and hence, the fit function is not smooth. Dually, the pseudo-entropy values of the high feature map are less concentrated. Given the vastness of the entropy values from the points on an embedded manifold, this would lead to a smooth translation function, and consequently, a smooth fit function. However, as will be shown, a highly expressible quantum feature map does not necessarily imply a strong relationship between the entropy of the data and the pseudo-entropy of the encoding scheme.

The following examples consist of binary classification with the quantum feature maps of either amplitude, angle, IQP, IQP SO, or IQP FL using the fidelity quantum kernel technique [1]. In all, the examples display an ambiguous relationship between the strength of the correlation coefficient and the performance of the statistical model trained with a quantum feature map. However, creating a method that gauges the performance of a model trained with an encoding scheme is quite difficult and intricate, requiring deep mathematical analysis that, intuitively, needs the entirety of the circuit for a complete analysis. In short, further empirical and mathematical analysis is required to extract information and formulate a relationship between pseudo-entropy and quantum model performance. Nevertheless, the results are quite interesting and may be used as a basis for the aforementioned empirical analysis.

The following examples consist of binary classification with the quantum feature maps of either amplitude, angle, IQP, IQP SO, or IQP FL using the fidelity quantum kernel technique [1]. In all, the examples display an ambiguous relationship between the strength of the correlation coefficient and the performance of the statistical model trained with a quantum feature map. However, creating a method that gauges the performance of a model trained with an encoding scheme is quite difficult and intricate, requiring deep mathematical analysis that, intuitively, needs the entirety of the circuit for a complete analysis. In short, further empirical and mathematical analysis is required to extract information and formulate a relationship between pseudo-entropy and quantum model performance. Nevertheless, the results are quite interesting and may be used as a basis for the aforementioned empirical analysis.

The following examples consist of binary classification with the quantum feature maps of either amplitude, angle, IQP, IQP SO, or IQP FL using the fidelity quantum kernel technique [1]. In all, the examples display an ambiguous relationship between the strength of the correlation coefficient and the performance of the statistical model trained with a quantum feature map. Of course, creating a mathematical relationship between entropy and pseudo-entropy mapping and quantum model performance is quite difficult.

In short, further empirical and mathematical analysis is required to extract information and formulate a relationship between pseudo-entropy and quantum statistical model performance. Nevertheless, the results are quite interesting and may be used as a basis for the aforementioned empirical analysis.

The first example comes from the Detect Ventricular Fibrillation [43], a Kaggle data set with a binary classification task. The data has fifty data points, four continuous features, and well-balanced labels. The ‘Freq.F’ feature was mapped to the unit interval with the sigmoid function and multiplied by 2π , the feature ‘Potencias’ was first normalized by dividing the points by 1,000,000, mapped with the sigmoid function and multiplied by 2π ,

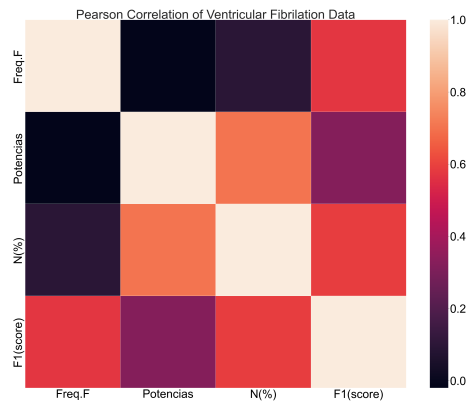


FIG. 11: These figures display a pattern between the entropies.

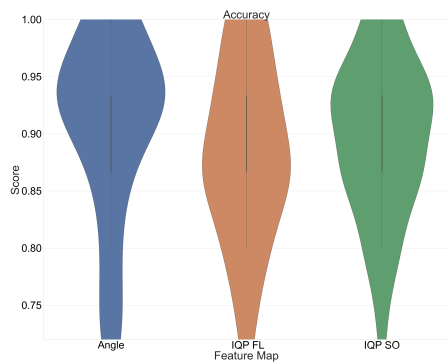
the feature ‘N(%)’ was divided by 100 and multiplied by 2π , and lastly, the feature ‘F1(score)’ was multiplied by 2π . Figure 11 shows the pairwise Spearman correlation coefficients of the features after the mappings.

For the experiments, for each of the quantum feature maps, thirty models are trained and an array of thirty seeds are applied to the 70/30-train/test split, for repeatable. The algorithm was the QSVC kernel algorithm in Qiskit [44]. Interestingly, Table II shows that the amplitude feature map and IQP feature map have the strongest relationship with the entropy of the data, but both encoding scheme had extremely poor performing models. However, the IQP SO feature map also has a strong relationship and trained models that performed quite well. The angle feature map trained models with the best performing models, but only had a mild nonlinear connection with the entropy of the data.

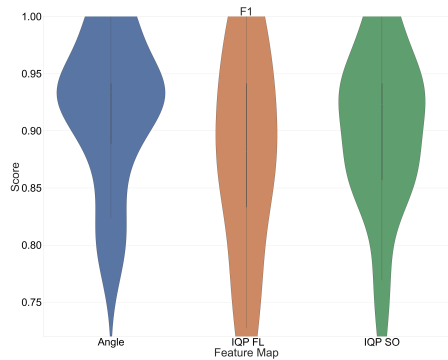
Correlations of Entropy and Pseudo-Entropy				
	Real Value		Modulus	
Feature Map	Spearman	Xicor	Spearman	Xicor
Amplitude	.5424	.2965	.5424	.2965
Angle	.0760	.2017	.0760	.2017
IQP	.3741	.1945	.2151	.1273
IQP FL	-.1637	.2245	-.3084	.0900
IQP SO	.3741	.1945	.2151	.1273

TABLE II: This table is the correlation coefficients of the Ventricular Fibrillation data set with the given encoding schemes.

The benchmarking analysis in Gennaro, Vlastic, and Pham [38] empirically displayed that the IQP has a higher expressibility than angle encoding, which is not surprising given the high level of entanglement created from correlation of the features within the IQP circuit. This higher expressibility score translated to more stable and robust quantum-based statistical models trained with IQP over the statistical models trained with the angle encoding scheme, although the models trained with



(a) The violin plot of the accuracy score.



(b) The violin plot of the f1 score.

FIG. 12: These figures display performance of the models trained on the Detect Ventricular Fibrillation data set with the angle, IQP FL, and IQP SO feature maps. The violin plots were cut off with the minimum and maximum values of the scores. The models trained with the Amplitude and IQP encoding scheme performed poorly and were not considered.

angle encoding did perform well. Contrarily, the amplitude feature map had an overall high expressibility score when compared to angle encoding but the statistical models trained with amplitude encoding performed poorly. This poor performance may stem from noise generated by the extra states.

From the Gennaro et al. paper, the entropy and pseudo-entropy of the Ionosphere dataset [45], where the subset of features are of that in [38], and the Sirtuin6 small molecules data set [46] are calculated. All of the features had the MaxAbsScaler in Scikit-learn [47] applied and fitted. Each data point is mapped to the 10-simplex or 6-simplex with the E diffeomorphic function in Equation 17. Following the experiments in [38], for the amplitude encoding scheme, $E(x)$ mapping is applied, for the angle encoding scheme, the map $2\pi \cdot E(x) - \pi$ is applied, and for the IQP encoding scheme, the map $2\pi \cdot E(x)$ is applied.

Table III shows a weak or relatively weak relationship with the pseudo-entropy of all of the quantum feature

maps and the entropy of both data sets, except for the angle feature map and the IQP FL encoding scheme on the Sirtuin6 data, though the IQP FL feature map was not considered in the analysis. As noted, the statistical models trained with the IQP encoding scheme were high-performing, but the correlation coefficients, at best, are weakly-related. The weak relationship with the IQP feature map and the data may stem from the low density of the sample of data points on the underlying embedded manifold.

As is repeatedly noted in the literature, particularly, Schuld, Sweke, and Meyer [4], data preparation has a large effect on the analysis. Ergo, on the values of the pseudo-entropy. Moreover, for our numerical experiments, we reduced the data dimensions so that they can be processed on simulator. This characteristic yields an improper representation of the embedded manifold that encompasses the data.

Correlations of Expressivity Example and Pseudo-Entropy				
Experiments		Real Value		Modulus
Data Set	Feature Map	Spearman	Xicor	Spearman Xicor
Sirtuin6	Amplitude	-.0824	.0402	-.0824 .0402
	Angle	-.8711	.5428	-.8711 .5428
	IQP	.0179	.0357	-.0066 .0936
	IQP FL	-.5770	.1815	-.5510 .2499
	IQP SO	.0179	.0357	-.0066 .0936
Ionosphere	Amplitude	-.2587	.1562	-.2587 .1562
	Angle	.9056	.6541	.9056 .6542
	IQP	.0686	.1716	.0263 .1235
	IQP FL	.0025	.1008	.0056 .1165
	IQP SO	.0686	.1716	.0263 .1253

TABLE III: Selected data sets from the experiments in de Luca et al. [38], the pseudo-entropy values are compared with the entropy of each respective data set.

Noise may be the cause for the poor performance of models trained with the amplitude encoding scheme. Hence, there is potential for a highly expressible encoding scheme to generate noise through the creation of quantum states that do not represent the latent information within the data. While globally the amplitude feature map has a high expressibility score, when the expressibility score was calculated locally, that is with respect to the given data, the expressibility score for amplitude was relatively low when compared to the angle feature map. Thanasilp, Wang, Cerezo, and Holmes [48] empirical show and claim that highly expressive encoding can lead to poor performance of the quantum kernel techniques through exponential concentration of values in the Graham matrix. This claim is emphasized by the amplitude feature map, however, the IQP feature map describe created highly performing quantum kernel models. Intuitively, the entirety of the circuit is required for a complete analysis Intriguingly, while the IQP encoding scheme had locally large expressibility scores, this technique had an extremely large global expressibility score, as previously noted, and outperformed all other quantum

statistical models, as well as being competitive against a top-of-class gradient boosted classifier.

V. DISCUSSION

This manuscript described a new and novel method to compare the ‘energy’ of a data point and the ‘energy’ of a given quantum feature map. Particularly, data points in a point-cloud are mapped to the simplex via a parameterless diffeomorphism and the entropy of each data point is calculated. For the quantum feature map, an analytic extension of von Neumann entropy, labeled as pseudo-entropy, is calculated for special unitary operator that represent the encoding scheme. For this unitary operator, von Neumann entropy is applied to the diagonal matrix of the eigenvalues. Since pseudo-entropy values are, in general, complex, a continuous map to the reals is applied in order to calculate the pseudo-entropy values to the entropy values.

The method is shown to be mathematically sound and argued to generalize two well-used techniques in QML, as well as argued to extended the symmetric encoding technique. However, deeper mathematical analysis is required to further support the claims generality. Furthermore, more empirical analysis and deeper categorical analysis is needed to understand the connection between the entropy of a point-cloud and the respective pseudo-entropy of a given quantum feature map.

One potential small fix to the shortcomings it to apply persistent homology [49, 50], and persistent entropy [51, 52] to the point-cloud to properly sample the data in order to compare entropy and pseudo-entropy through the approximation of the manifold the point-cloud represents. Of course, this approximation does not imply that the encoding technique will give an optimal result based on this formulation of information theoretic approach. As a result, further numerical testing on real dataset will be needed to connect the ansatz performance with the quantum information preservation.

Lastly, unlike expressivity and expressibility, a global phase factor has an effect on the pseudo-entropy values. To a lesser extent, empirical analysis and mathematical analysis is required to fully comprehend this effect.

The pseudo-entropy method is only one technique that considers information retention from the perspective of information theory, and as such, should not be considered as a standalone test. Furthermore, the perspectives of geometric structure and algebraic structure, to name a few, as information to be retained should be explored empirically and mathematically. The intersection of these

areas should yield deeper insight.

ACKNOWLEDGMENTS

I would like to thank Arthur Parzygnat and Anh Pham for all of their comments, suggested edits, and guidance throughout the creation of the idea and writing of this manuscript.

VI. DISCLAIMER

About Deloitte: Deloitte refers to one or more of Deloitte Touche Tohmatsu Limited (“DTTL”), its global network of member firms, and their related entities (collectively, the “Deloitte organization”). DTTL (also referred to as “Deloitte Global”) and each of its member firms and related entities are legally separate and independent entities, which cannot obligate or bind each other in respect of third parties. DTTL and each DTTL member firm and related entity is liable only for its own acts and omissions, and not those of each other. DTTL does not provide services to clients. Please see www.deloitte.com/about to learn more.

Deloitte is a leading global provider of audit and assurance, consulting, financial advisory, risk advisory, tax and related services. Our global network of member firms and related entities in more than 150 countries and territories (collectively, the “Deloitte organization”) serves four out of five Fortune Global 500® companies. Learn how Deloitte’s approximately 460,000 people make an impact that matters at www.deloitte.com. This communication contains general information only, and none of Deloitte Touche Tohmatsu Limited (“DTTL”), its global network of member firms or their related entities (collectively, the “Deloitte organization”) is, by means of this communication, rendering professional advice or services. Before making any decision or taking any action that may affect your finances or your business, you should consult a qualified professional adviser. No representations, warranties or undertakings (express or implied) are given as to the accuracy or completeness of the information in this communication, and none of DTTL, its member firms, related entities, employees or agents shall be liable or responsible for any loss or damage whatsoever arising directly or indirectly in connection with any person relying on this communication. Copyright © 2024 Deloitte Development LLC. All rights reserved.

[1] Vojtěch Havlíček, Antonio D Córcoles, Kristan Temme, Aram W Harrow, Abhinav Kandala, Jerry M Chow, and Jay M Gambetta. Supervised learning with quantum-enhanced feature spaces. *Nature*, 567(7747):209–212,

2019.

[2] Sukin Sim, Peter D Johnson, and Alán Aspuru-Guzik. Expressibility and entangling capability of parameterized quantum circuits for hybrid quantum-classical algo-

- rithms. *Advanced Quantum Technologies*, 2(12):1900070, 2019.
- [3] Israel F Araujo, Daniel K Park, Francesco Petruccione, and Adenilton J da Silva. A divide-and-conquer algorithm for quantum state preparation. *Scientific reports*, 11(1):1–12, 2021.
- [4] Maria Schuld, Ryan Sweke, and Johannes Jakob Meyer. Effect of data encoding on the expressive power of variational quantum-machine-learning models. *Physical Review A*, 103(3):032430, 2021.
- [5] Maria Schuld and Nathan Killoran. Quantum machine learning in feature hilbert spaces. *Physical review letters*, 122(4):040504, 2019.
- [6] Andrea Skolik, Jarrod R McClean, Masoud Mohseni, Patrick van der Smagt, and Martin Leib. Layerwise learning for quantum neural networks. *Quantum Machine Intelligence*, 3(1):1–11, 2021.
- [7] Michael J Bremner, Ashley Montanaro, and Dan J Shepherd. Average-case complexity versus approximate simulation of commuting quantum computations. *Physical review letters*, 117(8):080501, 2016.
- [8] Lov Grover and Terry Rudolph. Creating superpositions that correspond to efficiently integrable probability distributions. *arXiv preprint quant-ph/0208112*, 2002.
- [9] Hsin-Yuan Huang, Michael Broughton, Masoud Mohseni, Ryan Babbush, Sergio Boixo, Hartmut Neven, and Jarrod R McClean. Power of data in quantum machine learning. *Nature communications*, 12(1):1–9, 2021.
- [10] Andrew Vlasic and Anh Pham. Understanding the mapping of encode data through an implementation of quantum topological analysis. *Quantum Information and Computation*, 33(13 & 14):1091–1104, 2023.
- [11] Takahiro Goto, Quoc Hoan Tran, and Kohei Nakajima. Universal approximation property of quantum feature map. *arXiv preprint arXiv:2009.00298*, 2020.
- [12] Johannes Jakob Meyer, Marian Mularski, Elies Gil-Fuster, Antonio Anna Mele, Francesco Arzani, Alissa Wilms, and Jens Eisert. Exploiting symmetry in variational quantum machine learning. *PRX Quantum*, 4(1):010328, 2023.
- [13] Robert Ghrist. Barcodes: the persistent topology of data. *Bulletin of the American Mathematical Society*, 45(1):61–75, 2008.
- [14] Gunnar Carlsson and Mikael Vejdemo-Johansson. *Topological data analysis with applications*. Cambridge University Press, 2021.
- [15] Louis Schatzki, Andrew Arrasmith, Patrick J Coles, and Marco Cerezo. Entangled datasets for quantum machine learning. *arXiv preprint arXiv:2109.03400*, 2021.
- [16] John Lee. *Introduction to topological manifolds*, volume 202. Springer Science & Business Media, 2010.
- [17] José M Gracia-Bondía, Joseph C Várilly, and Héctor Figueroa. *Elements of noncommutative geometry*. Springer Science & Business Media, 2013.
- [18] Alain Connes. *Noncommutative geometry*. Springer, 1994.
- [19] A. Hatcher. *Vector Bundles and K-Theory*. 2003. <http://www.math.cornell.edu/~hatcher>.
- [20] Allen Hatcher. *Algebraic topology*. Cambridge University Press, Cambridge, 2002.
- [21] Shun-ichi Amari. *Information geometry and its applications*, volume 194. Springer, 2016.
- [22] Yoshifumi Nakata, Tadashi Takayanagi, Yusuke Taki, Kotaro Tamaoka, and Zixia Wei. New holographic generalization of entanglement entropy. *Phys. Rev. D*, 103(2):026005, 2021.
- [23] Michael A Nielsen and Isaac L Chuang. *Quantum computation and quantum information*. Cambridge university press, 2010.
- [24] Christoph Arndt. *Information measures: information and its description in science and engineering*. Springer Science & Business Media, 2001.
- [25] Marc Mezard and Andrea Montanari. *Information, physics, and computation*. Oxford University Press, 2009.
- [26] Jaap Van Oosten. *Basic category theory*. Citeseer, 1995.
- [27] Saunders Mac Lane. *Categories for the working mathematician*, volume 5. Springer Science & Business Media, 2013.
- [28] Emily Riehl. *Category Theory in Context*. Dover Publications, 2016.
- [29] John von Neumann. *Mathematical foundations of quantum mechanics: New edition*. Princeton university press, 2018.
- [30] Brian C Hall. *Quantum theory for mathematicians*. Springer, 2013.
- [31] Pauli Virtanen, Ralf Gommers, Travis E. Oliphant, Matt Haberland, Tyler Reddy, David Cournapeau, Evgeni Burovski, Pearu Peterson, Warren Weckesser, Jonathan Bright, Stéfan J. van der Walt, Matthew Brett, Joshua Wilson, K. Jarrod Millman, Nikolay Mayorov, Andrew R. J. Nelson, Eric Jones, Robert Kern, Eric Larson, C J Carey, İlhan Polat, Yu Feng, Eric W. Moore, Jake VanderPlas, Denis Laxalde, Josef Perktold, Robert Cimrman, Ian Henriksen, E. A. Quintero, Charles R. Harris, Anne M. Archibald, Antônio H. Ribeiro, Fabian Pedregosa, Paul van Mulbregt, and SciPy 1.0 Contributors. SciPy 1.0: Fundamental Algorithms for Scientific Computing in Python. *Nature Methods*, 17:261–272, 2020.
- [32] Yoshifumi Nakata, Tadashi Takayanagi, Yusuke Taki, Kotaro Tamaoka, and Zixia Wei. Holographic pseudo entropy. *arXiv preprint arXiv:2005.13801*, 2020.
- [33] Alexei Kitaev and John Preskill. Topological entanglement entropy. *Physical review letters*, 96(11):110404, 2006.
- [34] Craig S Lent. Quantum operator entropies under unitary evolution. *Physical Review E*, 100(1):012101, 2019.
- [35] Tatzuma Nishioka, Tadashi Takayanagi, and Yusuke Taki. Topological pseudo entropy. *Journal of High Energy Physics*, 2021(9):1–44, 2021.
- [36] Jyotirmoy Mukherjee. Pseudo entropy in $u(1)$ gauge theory. *Journal of High Energy Physics*, 2022(10):1–30, 2022.
- [37] Yoshifumi Nakata, Tadashi Takayanagi, Yusuke Taki, Kotaro Tamaoka, and Zixia Wei. New holographic generalization of entanglement entropy. *Physical Review D*, 103(2):026005, 2021.
- [38] Gennaro De Luca, Andrew Vlasic, Michael Vitz, and Anh Pham. Empirical power of quantum encoding methods for binary classification. *arXiv preprint arXiv:2408.13109*, 2024.
- [39] Y Dodge. *The Concise Encyclopedia of Statistics*. Springer New York, 2008.
- [40] Hans-Otto Georgii. *Gibbs measures and phase transitions*. Walter de Gruyter GmbH & Co. KG, Berlin, 2011.
- [41] Veeravalli S Varadarajan. *Lie groups, Lie algebras, and their representations*, volume 102. Springer Science & Business Media, 2013.
- [42] Sourav Chatterjee. A new coefficient of correla-

- tion. *Journal of the American Statistical Association*, 116(536):2009–2022, 2021.
- [43] Detect Ventricular Fibrillation metrics file <https://www.kaggle.com/datasets/rubenbaeza/fibrilaao>.
- [44] Gadi Aleksandrowicz, Thomas Alexander, Panagiotis Barkoutsos, Luciano Bello, Yael Ben-Haim, David Bucher, F Jose Cabrera-Hernández, Jorge Carballo-Franquis, Adrian Chen, Chun-Fu Chen, et al. Qiskit: An open-source framework for quantum computing. *Accessed on: Mar*, 16, 2019.
- [45] V. Sigillito, S. Wing, L. Hutton, and K. Baker. Ionsphere. UCI Machine Learning Repository, 1989. DOI: <https://doi.org/10.24432/C5W01B>.
- [46] Mehmet Tardu and Fatih Rahi. Sirtuin6 Small Molecules. UCI Machine Learning Repository, 2022. DOI: <https://doi.org/10.24432/C56C9Z>.
- [47] Fabian Pedregosa, Gaël Varoquaux, Alexandre Gramfort, Vincent Michel, Bertrand Thirion, Olivier Grisel, Mathieu Blondel, Peter Prettenhofer, Ron Weiss, Vincent Dubourg, et al. Scikit-learn: Machine learning in python. *the Journal of machine Learning research*, 12:2825–2830, 2011.
- [48] Supanut Thanasilp, Samson Wang, M Cerezo, and Zoë Holmes. Exponential concentration in quantum kernel methods. *Nature Communications*, 15(1):5200, 2024.
- [49] Nina Otter, Mason A Porter, Ulrike Tillmann, Peter Grindrod, and Heather A Harrington. A roadmap for the computation of persistent homology. *EPJ Data Science*, 6:1–38, 2017.
- [50] Michael J Catanzaro and Brantley Vose. Harmonic representatives in homology over arbitrary fields. *Journal of Applied and Computational Topology*, 7(3):643–670, 2023.
- [51] Harish Chintakunta, Thanos Gentimis, Rocio Gonzalez-Diaz, Maria-Jose Jimenez, and Hamid Krim. An entropy-based persistence barcode. *Pattern Recognition*, 48(2):391–401, 2015.
- [52] Emanuela Merelli, Matteo Rucco, Peter Slood, and Luca Tesei. Topological characterization of complex systems: Using persistent entropy. *Entropy*, 17(10):6872–6892, 2015.